Data-driven modeling of nonlinear materials in normal-conducting magnets

Stefano Sorti,* Carlo Petrone, and Stephan Russenschuck
CERN, European Organization for Nuclear Research, CH-1211 Geneva 23, Switzerland

Francesco Braghin
Politecnico di Milano, Dipartimento di Meccanica, via La Masa 1, 20156 Milano, Italy

(Received 1 October 2021; accepted 25 April 2022; published 27 May 2022)

Accurate numerical modeling of normal-conducting accelerator magnets requires a reliable characterization of the iron saturation and hysteresis as well as a precise knowledge of the magnet geometry as built. Computations of the field quality are not easily achieving the accuracy required by the accelerator operation, particularly for eddy-current effects in fast-ramping magnets. This paper proposes a (measurement) data-driven model for the nonlinear magnetization of normal-conducting magnets. The model adopts a volume integral formulation compatible with eddy-current simulations. A two-step updating procedure is applied. The first step is the fitting of material parameters directly in the magnet model. The second step is the updating of the magnetization by measurements of the integral field harmonics. The result is a full-order updated model that can be employed in static or dynamic simulations. Finally, the procedure is validated on an iron-dominated, normal-conducting magnet.

DOI: 10.1103/PhysRevAccelBeams.25.052401

I. INTRODUCTION

Magnets are used in particle accelerators to deflect and focus particle beams. Depending on the needs, electromagnets come in a variety of designs, with different materials, geometries, and sizes [1]. The fundamental distinction is between iron-dominated, normal-conducting magnets and coil-dominated, superconducting magnets. Another classification is the magnet's optical function on the particle beam (bending, focusing, or chromaticity correction), leading to different field distributions (dipole, quadrupole, sextupole, and higher-order harmonics). Because of the saturation magnetization of iron, superconducting magnets are often the only option when fields larger than 2 T are required. In general, normal-conducting magnets allow faster ramp rates, even of the order of thousands of Tesla per second (like septum magnets), and do not require the operation of a cryogenic system. A review of the topic can be found in Ref. [2].

Most normal-conducting magnets are iron dominated, which implies that the field quality is defined by the shape of the iron pole. The uncertainties in the simulation of nonlinear electromagnetic fields are often larger than the requirements for beam operation. Additional sources of uncertainty are intrinsic errors in model assumptions, approximation errors caused by domain finite-element discretization, coupled phenomena such as thermal and mechanical effects (magnetostriction), and transient fields by eddy currents [3].

As a result, magnetic measurements are typically required. They can ensure an accuracy better than 10^{-4}, relative to the main integral field [4]. However, measurements are affected by spatial and temporal resolution limitations as well as the need for application-specific transducers [5], as no single transducer exists for all quantities to be measured. Moreover, for magnets already placed in accelerators, only parts of the aperture may be accessible due to auxiliary equipment.

Simulations and measurements are, therefore, both limited but complementary in the field description of magnets. The former offer virtually no limits in terms of evaluation conditions, while the latter guarantee a sufficient accuracy level. The idea behind data-driven modeling is, therefore, to construct a numerical model that is updated by magnetic measurements. The ideal result is a model that preserves its physical properties

*stefano.sorti@polimi.it; stefano.sorti@cern.ch
Also at Politecnico di Milano, Dipartimento di Meccanica, via La Masa 1, 20156 Milano, Italy.

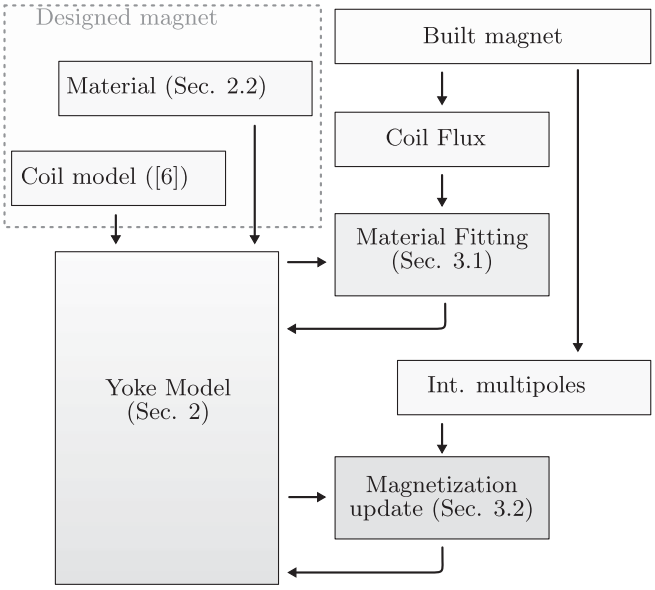

FIG. 1. Flow chart of the proposed data-driven modeling.

while matching the experimental results within the required accuracy.

In this paper, we propose a data-driven model for static magnetization of nonlinear iron yokes. We adopt an integral formulation with 18 degrees-of-freedom (d.o.f.) elements. In this way, a straightforward coupling with the eddy-current model in Ref. [6] is possible. The data-driven correction first addresses the identification of material parameters, while the second part of the process involves the updating of the static magnetization. The integrated field harmonics in the magnet aperture are measured, and the magnetization distribution is updated to match these measurements. Despite the use of integral measurements only, the procedure enhances the model accuracy even in the local field distribution, as has been verified experimentally. The outcome of the procedure is a full-order model of the iron magnetization, which can be employed for magnetostatic evaluations or coupled with eddy-current calculations. A flow chart of the procedure is shown in Fig. 1.

A. Data-driven updating of models

Improving the accuracy of numerical models through measurements is not a new idea. Earlier attempts aimed at parameter estimation for lumped circuits and later for distributed models [7]. The updates of FEM models is particularly common in mechanical engineering, and it has provided relevant progresses for the topic [8–10]. The goal of these *model-updating* methods is to optimize the entries of the linear mass and stiffness matrices to reduce the discrepancy between measured and computed eigenmodes of the system [11]. With more demanding applications, some issues have arisen, such as the quantification of uncertainty in the measured data (introducing the so-called Bayesian updating [12,13]) and the need for a continuous, online update of the model [14]. These aspects can be further combined in a stochastic estimation of both model parameters and system state [15]. Bayesian methodology is widely adopted for ill-posed problems, as an alternative to classical regularization techniques [16]. Some of these aspects have yet to be investigated for the operation of particle accelerator magnets, and the presented work aims at being a step in this direction.

The problem of data-driven updating for magnetic devices is typically related to the *field reconstruction* problem. This class of problems starts with a prescribed magnetic model (the *prior*), whose unknowns in the form of parameters or system states must be identified by magnetic field measurements.

The specific application to particle accelerator magnets has been presented for a 2D model in Refs. [17,18] and for a 3D problem in Ref. [19]. These methods increase the accuracy of the field reconstruction, as they include a model for noise and uncertainties by adopting stochastic methods. However, these methods show limited extrapolation properties, because the models are not fully reproducing the real device. The prior is often an equivalent model rather than a physical one.

The authors of this paper have already contributed to the topic in Ref. [6] by a model-updating method for a 3D physical model of magnets. This attempt, however, suffered from three main limitations. (1) Nonlinear magnetic materials are excluded; (2) devoted measurement campaigns are required; and (3) the updated model is of reduced order only. This paper proposes a method that overcomes these limitations. It focuses on nonlinear materials only, so it is crucial that the updated model remains open to further manipulations, such as a subsequent coupling with eddy-current models. This required the updated model be of full order. The method is specifically devoted to accelerator magnets, so that it can exploit standard magnetic measurements. The proposed method is, therefore, not adopting statistical inference.

The novelty of this work is, therefore, a first complete procedure of model updating for accelerator magnets, with no cost in terms of required measurements and limited cost in computations.

II. THE PHYSICAL MODEL

The model of the excitation coil employs 3D brick elements, in which the current direction is fixed, but the current density can vary on the cross section. The magnetic field, generated by the coil, is computed by the Biot-Savart law for both the calculation of the magnetization in the yoke elements and the calculation of the quantities to be acquired by magnetic measurements. Details of the model can be found in Ref. [6].

The formulation for iron magnetization is based on the computation of the magnetic field $\mathbf{H}$ generated by a

magnetized volume $\mathscr{V}'$ (the source) in a region of space identified as $\mathscr{V}$ (the target). For this purpose, the scalar potential for the magnetization is introduced [20–22]:

$$\mathbf{H}=\mathbf{H}_{\mathrm{M}}+\mathbf{H}_{\mathrm{S}}=-\frac{1}{4\pi}\nabla\underbrace{\int_{\mathscr{V}'}\mathbf{M}\nabla'\frac{1}{r}\mathrm{dV}'}_{\phi_{\mathrm{M}}}+\mathbf{H}_{\mathrm{S}}$$
$$=-\frac{1}{4\pi}\nabla\left[-\int_{\mathscr{V}'}\frac{\nabla'\cdot\mathbf{M}'}{r}\mathrm{dV}'+\int_{\mathscr{A}'}\frac{\mathbf{M}'\cdot\mathbf{n}'}{r}\mathrm{dA}'\right]+\mathbf{H}_{\mathrm{S}}, \quad (1)$$

where $\mathbf{H}_M$ and $\mathbf{H}_S$ are the contributions from the magnetization and external sources, respectively. To save on notation, we denote by r the distance between the source point and the field (target) point. The constitutive equations for the magnetic materials are, thus, written in the form $\mathbf{M}=\chi\mathbf{H}$ and enforced on the left side of the equation. For the field generated by the excitation coils, it is possible to express $\mathbf{H}_{\mathrm{S}}=\mathbf{H}_{\mathrm{S}}(\boldsymbol{I})$, where $\boldsymbol{I}$ are the currents in the coil elements.

A. Weak formulation and shape functions

In order to express Eq. (1) in a weak formulation, we write $\mathbf{M}=\sum\boldsymbol{w}_k(\boldsymbol{r})M_k(t)$, with vector shape functions $\boldsymbol{w}_k(\boldsymbol{r})$. The roman type ($\mathbf{M}$) identifies local quantities, while the italic type ($\boldsymbol{M}$) denotes the model degrees of freedom. Giving elements j and k and weights $\boldsymbol{p}_j$, it yields

$$\begin{aligned}
&\int_{\mathscr{V}}\frac{\boldsymbol{p}_j\cdot\boldsymbol{w}_j}{\chi}\mathrm{dV}\,M_j\\
&=-\frac{1}{4\pi}\int_{\mathscr{V}}\int_{\mathscr{V}'}\frac{(\nabla\cdot\boldsymbol{p}_j)(\nabla'\cdot\boldsymbol{w}_k')}{r}\mathrm{dV}'\mathrm{dV}M_k\\
&\quad+\frac{1}{4\pi}\int_{\mathscr{A}}\int_{\mathscr{V}'}\frac{(\boldsymbol{p}_j\cdot\boldsymbol{n})(\nabla'\cdot\boldsymbol{w}_k')}{r}\mathrm{dV}'\mathrm{dA}M_k\\
&\quad+\frac{1}{4\pi}\int_{\mathscr{V}}\int_{\mathscr{A}'}\frac{(\boldsymbol{w}_k'\cdot\boldsymbol{n}')(\nabla\cdot\boldsymbol{p}_j)}{r}\mathrm{dA}'\mathrm{dV}M_k\\
&\quad-\frac{1}{4\pi}\int_{\mathscr{A}}\int_{\mathscr{A}'}\frac{(\boldsymbol{p}_j\cdot\boldsymbol{n})(\boldsymbol{w}_k'\cdot\boldsymbol{n}')}{r}\mathrm{dA}'\mathrm{dA}M_k+\int_{\mathscr{V}'}\boldsymbol{p}_j\cdot\mathbf{H}_{\mathrm{S}}\mathrm{dV}.
\end{aligned} \quad (2)$$

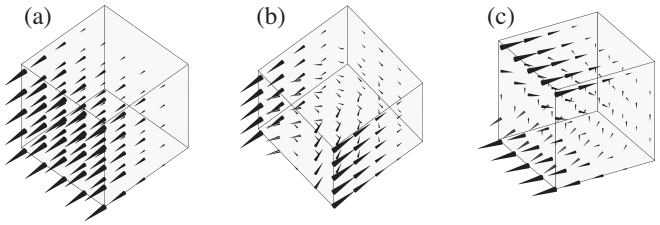

FIG. 2. The three shape functions per face proposed for the iron magnetization: the facet function (a) and the two recirculating functions (b) and (c).

If χ is constant, it is possible to write the matrix equation

$$[D]\boldsymbol{M}=[E]\boldsymbol{M}+[F]\boldsymbol{I}. \quad (3)$$

The main rationale in the selection of shape functions is the treatment of singular integrals. Zero-order shape functions are commonly used in the literature [23–25]; that is, each element is modeled as a brick with a consistent magnetization. Because of the constant flux through surface elements and divergence-free properties, analytical solutions for integrals are possible [6].

Alternatives have been proposed, such as facet shape functions, also called lowest-order Raviart-Thomas elements [26–28], often employed for formulations in $\mathbf{H}$ [29,30]. One facet shape function is shown in Fig. 2(a). Facet functions exhibit constant flux through surface elements and constant divergence; thus, their integrals can be solved like the ones for elements with zero-order shape functions.

However, facet elements cannot represent linear variations in any direction of the element; therefore, additional shape functions are introduced. This set of functions are known as recirculating shape functions and their elements as Brezzi-Douglas-Marini elements of the first order [31]. To the authors' knowledge, they have not been employed in magnetic field problems yet. Recirculating shape functions provide a divergence-free, linearly varying field on the surfaces. These properties simplify the solution of the integrals in Eq. (2), so that almost the same schemes adopted for zero-order and facet shape functions can be

TABLE I. Shape functions for the yoke elements. Facet functions (first column) and recirculating functions (second and third columns).

$\boldsymbol{w}_{1,i}(s_1,s_2,s_3)$	$\boldsymbol{w}_{2,i}(s_1,s_2,s_3)$	$\boldsymbol{w}_{3,i}(s_1,s_2,s_3)$
$[s_1/8-1/8,0,0]$	$[2s_2(s_1-1),1-s_2^2,0]$	$[-2s_3(s_1-1),0,s_3^2-1]$
$[s_1/8+1/8,0,0]$	$[-2s_2(s_1+1),s_2^2-1,0]$	$[2s_3(s_1+1),0,1-s_3^2]$
$[0,s_2/8-1/8,0]$	$[s_1^2-1,-2s_1(s_2-1),0]$	$[0,2s_3(s_2-1),1-s_3^2]$
$[0,s_2/8+1/8,0]$	$[1-s_1^2,2s_1(s_2+1),0]$	$[0,-2s_3(s_2+1),s_3^2-1]$
$[0,0,s_3/8-1/8]$	$[1-s_1^2,0,2s_1(s_3-1)]$	$[0,s_2^2-1,-2s_2(s_3-1)]$
$[0,0,s_3/8+1/8]$	$[s_1^2-1,0,-2s_1(s_3+1)]$	$[0,1-s_2^2,2s_2(s_3+1)]$

applied; see the Appendix. Recirculating shapes are shown in Fig. 2 and listed in Table I.

B. Nonlinear materials

Dealing with nonlinear materials, it is convenient to rewrite Eqs. (1) and (2) in differential form, so that the unknowns of the problem become $\mathrm{d}\boldsymbol{M}$. This is done considering Eq. (1) as $\Delta\mathbf{H} = \Delta\mathbf{H}_{\mathrm{M}}(\Delta\mathbf{M}) + \Delta\mathbf{H}_{\mathrm{S}}$, for arbitrary small Δ. The constitutive relations must, therefore, be rewritten accordingly: The scalar susceptibility χ is replaced by a matrix $[\chi_{\mathrm{d}}] = \mathrm{d}\mathbf{M}/\mathrm{d}\mathbf{H}$. The right-hand side of the new equation becomes

$$\int_{\mathscr{V}} \boldsymbol{p}_j [\chi_{\mathrm{d}}]^{-1} \boldsymbol{w}_j \mathrm{d}V \mathrm{d}M_j. \tag{4}$$

In case of an isotropic material, simpler expressions result from the scalar relationship between absolute values as $|\mathbf{M}| = \chi(|\mathbf{H}|)|\mathbf{H}|$. A first approximation is to consider the diagonal-only entries in $[\chi_{\mathrm{d}}]$, which is also part of a vector-hysteresis model, of interest for future developments of the proposed method [32]. A further step is to identify $\chi_{\mathrm{d}} = \mathrm{d}|\mathbf{M}|/\mathrm{d}|\mathbf{H}|$, employing it as a *unidirectional* differential susceptibility, further simplifying the computations at the cost of a loss in accuracy [33]. This latter has provided satisfactory results for our applications.

Manipulating Eq. (3), we write for the general case

$$\underbrace{[D^{(\mathrm{L})}][\chi_{\mathrm{d}}(\boldsymbol{r})]^{-1}_{i,j}[D^{(\mathrm{R})}]}_{[D(\mathbf{H}(\boldsymbol{r}))]} \mathrm{d}\boldsymbol{M} = [E]\mathrm{d}\boldsymbol{M} + [F]\mathrm{d}\boldsymbol{I}. \tag{5}$$

The only term that changes with respect to the linear case is the matrix $[D]$. This matrix is to be reassembled at each step and consists of three terms. The central one is the diagonal block matrix containing the 3×3 inverse of the differential susceptibility in the N_{G} Gauss points adopted for integration of $[D]$. The matrices $[D^{(\mathrm{L})}]$ and $[D^{(\mathrm{R})}]$ contain the remaining terms to assemble $[D]$. They have dimensions $W \times 3N_{\mathrm{G}}$ and $3N_{\mathrm{G}} \times W$, respectively, where W is the size of vector $\boldsymbol{M}$. $[D^{(\mathrm{L})}]$ and $[D^{(\mathrm{R})}]$ are sparse, and, therefore, reassembly is fast to perform.

Differential permeability elements can be computed in several ways. The direct approach is to compute $\mathbf{H}$ pointwise by Eq. (1) but dealing with singular integrals. If the materials remain relatively far from saturation, $\mathbf{H}$ could be also expressed in a weak form (introducing $\boldsymbol{H}$) and interpolated with the same shape functions of $\mathbf{M}$. This may not be the case for most magnets, however. A faster approach, for unidirectional susceptibility, it is to employ $\chi_{\mathrm{d}}\{\chi^{-1}[\mathbf{M}(\boldsymbol{r})]\}$, so that $\mathbf{M}$ is computed in the Gauss points by shape functions and the constitutive equation is enforced locally.

When the iron saturates, $\chi_{\mathrm{d}} \to 0$, so the first term in Eq. (5) becomes singular. A practical solution is to impose a reasonably low boundary to χ_{d} (like 10^{-5}) to preserve the numerical stability or not to integrate the d.o.f. with a too small χ_{d}. The other option, which is reassembling matrices $[E]$ and $[F]$, is discouraged, because it involves fully populated matrices.

Equation (5) can be solved explicitly for $\mathrm{d}\boldsymbol{M}$. Once the matrix $[D] - [E]$ is computed, its symmetry and positive-definiteness can be exploited by a Cholesky decomposition, so that triangular solvers can subsequently be adopted. Adaptive-step time integrators are then suggested [such as ode45() in MATLAB®].

If analytical expressions are employed for χ_{d}, the empirical Wlodarski curve [34,35] is typically an acceptable approximation [1]:

$$\mathrm{M}(\mathrm{H}) = \mathrm{M_a} L\left(\frac{\mathrm{H}}{a}\right) + \mathrm{M_b} \tanh\left(\frac{|\mathrm{H}|}{b}\right) L\left(\frac{\mathrm{H}}{b}\right), \tag{6}$$

$$\text{where } L\left(\frac{\mathrm{H}}{a}\right) \coloneqq \coth\left(\frac{\mathrm{H}}{a}\right) - \left(\frac{a}{\mathrm{H}}\right), \tag{7}$$

and M_{a}, M_{b}, a, and b are parameters, while M and H are the magnitude of magnetization and magnetic field in the given point of the material, respectively.

III. DATA-DRIVEN CORRECTION OF THE MODEL

Three sources of uncertainty can be identified in normal-conducting accelerator magnets: the material properties, the shape of the yoke, and the characteristics of the coils [36]. The proposed procedure covers two of the three—material properties and yoke geometry—as the coil is already discussed in Ref. [6]. For each source of uncertainty, an independent procedure is proposed in the next subsections. Their order is not mandatory: Depending on the specific need, each step can be avoided, or iterated after the other, guaranteeing flexibility of the process.

Two constraints for the procedure are imposed *a priori*: (i) *Relying on integral field measurements only, so that the acquisition of experimental data corresponds to a typical magnet characterization.*—This is consistent with the statement that, in most cases, integral-field multipoles are sufficient to characterize a magnet [1]. (ii) *Employ methods which preserve the full order of the model.*—This is needed for a subsequent coupling with eddy-current models.

As a final remark, the proposed procedure considers only one excitation coil, so that the term $[F]\mathrm{d}\boldsymbol{I}$ in Eq. (5) becomes $\mathbf{F}\mathrm{d}I$.

A. Parameter fitting for magnetic materials

This section presents a procedure for fitting M(H) curve parameters, employing magnetic measurements of the magnet. Typically, magnetic measurements of materials are performed for specimens with well-defined field distribution, like in ring-sample permeameters, and without burrs, welding seams, and any other critical features on the material [37]. The results are then provided as an input for magnet simulations [1].

Dealing with magnetic measurements of production magnets, it may be impossible to distinguish the effects of the yoke geometry and magnetic material characteristics on the measured field quality. The proposed procedure relies on the measurement of the overall flux linked with the excitation coil: The voltage V and the current I across the excitation coils are measured, while the resistance R is characterized. This yields

$$\phi(t) = \int [V(t) - R(T,t)I(t)]\mathrm{d}t, \tag{8}$$

where T is the temperature. This approach aims at obtaining a global measurement, averaging out local defects. Similar approaches have been successfully proposed for electric motors [38,39].

We, therefore, identify the experimental and modeled steady-current fluxes $\phi(I)_\mathrm{X}$ and $\phi(I)_\mathrm{M}$ and get

$$J(\boldsymbol{p}) = \int_{I_1}^{I_2} |\phi(I)_\mathrm{X} - \phi(I,\boldsymbol{p})_\mathrm{M}|\mathrm{d}I, \tag{9}$$

to be computed numerically between the minimum and maximum currents I_1 and I_2. Vector $\boldsymbol{p}$ contains the material parameters, to be obtained by minimizing $J(\boldsymbol{p})$. Adopting Eq. (6), four parameters are required. The optimization problem can be solved with standard gradient-based tools [such as fmincon() in the MATLAB® optimization toolbox].

An additional step is proposed to speed up the process, by employing a parametric, reduced-order model through proper orthogonal decomposition with interpolation [40–42]. For a full account of this technique, the reader is referred to Refs. [43,44]. The full model is evaluated for $[I_1, I_2]$ at the $2^4 = 16$ vertices of the 4D parameter domain $[\mathrm{a}_1,\mathrm{a}_2]\times[\mathrm{b}_1,\mathrm{b}_2]\times[\mathrm{M}_{\mathrm{a},1},\mathrm{M}_{\mathrm{a},2}]\times[\mathrm{M}_{\mathrm{b},1},\mathrm{M}_{\mathrm{b},2}]$. Proper orthogonal decomposition is employed, with the same snapshot and mode selection. A set of $\hat{\boldsymbol{\Psi}}_i$ reduction bases is obtained, with $i \in [1, 16]$. A reduced basis for any combination of parameters inside the domain is constructed with a quadrilinear interpolation $\boldsymbol{\Psi}(\boldsymbol{p}) = \sum \alpha_i(\boldsymbol{p})\hat{\boldsymbol{\Psi}}_i$, where $\alpha_i(\boldsymbol{p})$ are the interpolation coefficients. The optimization routine, before computing Eq. (9), reduces the model through the basis $\boldsymbol{\Psi}(\boldsymbol{p})$, leading to a relevant gain in computation time.

B. Model updating of the magnetization

The updating of the magnetization model aims at reducing the error between the computed and measured fields. As already discussed in Sec. I A, we may interpret this step as a field reconstruction problem. Common approaches, eventually also adopting an integral formulation [45], solve a problem of the form $[C_\mathrm{m}]\mathbf{M} = \boldsymbol{\mathcal{C}}$, where $[C_\mathrm{m}]$ is the fully populated matrix expressing the simulated pointwise measurements as a function of the model magnetization $\mathbf{M}$ and where $\boldsymbol{\mathcal{C}}$ is the measurement result.

The magnetic measurements to be exploited in this procedure are, as said, integral multipoles from rotating-coil magnetometers—more specifically, the subset of the K relevant multipoles. Measurements are simulated as in Ref. [6], where the vector potential from the sources is integrated over the coil profile. The output matrix $[C_\mathrm{m}] \in \mathrm{IR}^K \times \mathrm{IR}^W$, where W is the size of $\boldsymbol{M}$, is constructed. The simulated profiles of the $N - K$ multipoles that are not subjected to the updating are collected in the tensor $[C_\mathrm{p}] \in \mathrm{IR}^{(N-K)} \times \mathrm{IR}^P \times \mathrm{IR}^W$, where P is the number of points chosen to discretize the profiles in the axial direction. This tensor is later employed to guarantee the updating phase is not altering the higher-order harmonics.

Given the characteristics of $[C_\mathrm{m}]$, where $W \gg K$, it is easy to assess that the problem $[C_\mathrm{m}]\boldsymbol{M} = \boldsymbol{\mathcal{C}}$ is strongly undetermined. We, thus, propose another approach, with two main changes to the problem. First, we take $\Delta\boldsymbol{M}$, variations of the magnetization with respect to the outcome of the model, as "design" variables. Consistently, we evaluate the error between the simulated and the measured multipoles $\Delta\mathcal{C}$. The field reconstruction becomes, thus, a field correction, where the largest contribution is expected to come from the physical model. The aim is to find the correction that has the minimum impact on the model, thus preserving its physical relevance. We thus write

$$\begin{aligned} &\min_{\Delta\mathbf{M}} \frac{1}{2}\Delta\boldsymbol{M}^\mathrm{T}[Q]\Delta\boldsymbol{M} \\ &\text{subject to} \begin{bmatrix} C_\mathrm{m} \\ C_\mathrm{p} \end{bmatrix} \Delta\mathbf{M} = \begin{bmatrix} \Delta\boldsymbol{\mathcal{C}} \\ 0 \end{bmatrix}, \end{aligned} \tag{10}$$

where $\sqrt{Q_{j,j}} = \frac{V_j}{\sum V_j M_{i,j}}$ and V_j is the jth volume element of the magnetic material. Matrix $[Q]$ is, therefore, a weighting matrix, so that each ΔM_i is weighted by its effect on the magnetized volume.

The overall procedure is, thus, as follows. (1) The matrices $[C_\mathrm{m}]$ and $[C_\mathrm{p}]$ are assembled once for all, based on the magnetic measurements. (2) The set of current values L at which measurements are available is taken, with $I_i \in L$. The model from Eq. (5) is solved on L, returning a set of $[\boldsymbol{M}_i(I_i), I_i]$. (3) Optimization of Eq. (10) is performed $\forall\, I_i$. Being a quadratic programming process, the solution is unique and appropriate tools are available [such as quadprog() in MATLAB®]. The solutions $\Delta\boldsymbol{M}_i(I_i)$ are

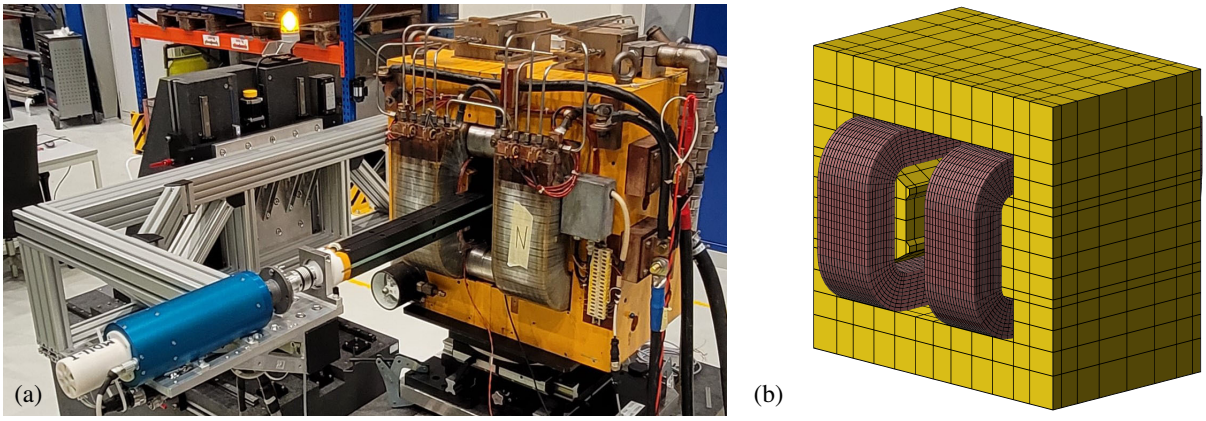

FIG. 3. The MDX magnet on the measurement system (a) and the mesh of the model (b).

interpolated with a spline over L, to write $\Delta\boldsymbol{M}(I)$. (4) The correction is implemented in model equations by an additional magnetization input $\Delta\boldsymbol{F}(I)$, so that the updated model (u) returns $\boldsymbol{M}_{\mathrm{u}}(I) = \boldsymbol{M}(I) + \Delta\boldsymbol{M}(I)$. The last step is done by integrating into I the equation

$$\{D[\mathbf{H}_{\mathrm{u}}(\boldsymbol{r})]\}\mathrm{d}\boldsymbol{M}_{\mathrm{u}}(I) = [E]\mathrm{d}\boldsymbol{M}_{\mathrm{u}}(I) + [\boldsymbol{F} + \Delta\boldsymbol{F}(I)]\mathrm{d}I, \quad (11)$$

after explicating $\Delta\boldsymbol{F}(I)$ from the right-hand side. The choice of updating vector $\boldsymbol{F}(I)$ comes from the need for preserving the symmetry and positive-definiteness of $[D]$, $[E]$, and $[D] - [E]$. If the updating affects fully saturated parts of the yoke, some terms in $\Delta\boldsymbol{F}(I)$ may become very large. It is then suggested to impose $\Delta\boldsymbol{F}(I) = \Delta\boldsymbol{F}(I_{\mathrm{lim}})$ for a reasonable threshold $I > I_{\mathrm{lim}}$. This slightly reduces the updating performance at saturation, highlighting the importance of a reliable material updating from Sec. III A.

The proposed approach does not involve additional physical parameters, such as geometric features or dimensions, but is nevertheless sensitive to geometrical errors. The proposed method can provide a first insight on where the most relevant defects may be located: The regions where $\Delta M_{i,j}/M_{i,j}$ is highest are of interest for further investigation of the real device. Once a discrepancy between the design-based model and the real device is identified in the mechanics, the model may be adjusted accordingly.

TABLE II. Fitting for Wlodarski curve [Eq. (6)] to MDX.

A/m	Initial values	Range	Final values
M_{a}	1.347×10^6	±25%	1.588×10^6
a	452.2	±50%	623.6
M_{b}	0.3197×10^6	±50%	0.252×10^6
b	8090	±50%	9175

IV. EXPERIMENTAL VALIDATION

The device used for the experimental validation of the method is a skew dipole called MDX, previously installed in the East area of the CERN accelerator complex [46]. The MDX magnets have an adjustable aperture size; in our case, it is 148 mm. The magnet mounted on the measurement bench [47] is shown in Fig. 3(a); the mesh of the model is shown in Fig. 3(b). The coil model consists of 35 657 elements, with 62 413 d.o.f. (before model-order reduction [6]). The yoke is discretized into 992 elements resulting in 10 596 d.o.f.

The yoke is made of solid blocks of AISI 1010 steel. Different permeability curves for this material are available in Ref. [48], and the one used in the software OPERA® is adopted (later identified by the letter a). This allows us to compare our results with the existing simulations and measurements of the magnet, in order to guarantee an acceptable starting point for the nonupdated model. On a

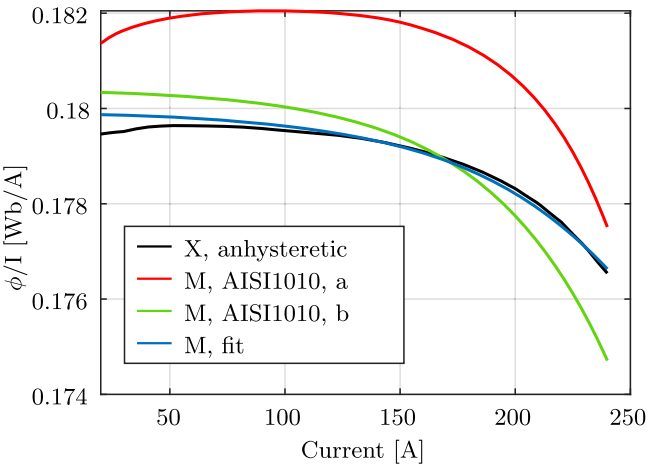

FIG. 4. Parameter fitting for the Wlodarski iron magnetization curve [Eq. (6)]. Excitation coil flux is reported for measurements and for the different stages of fitting.

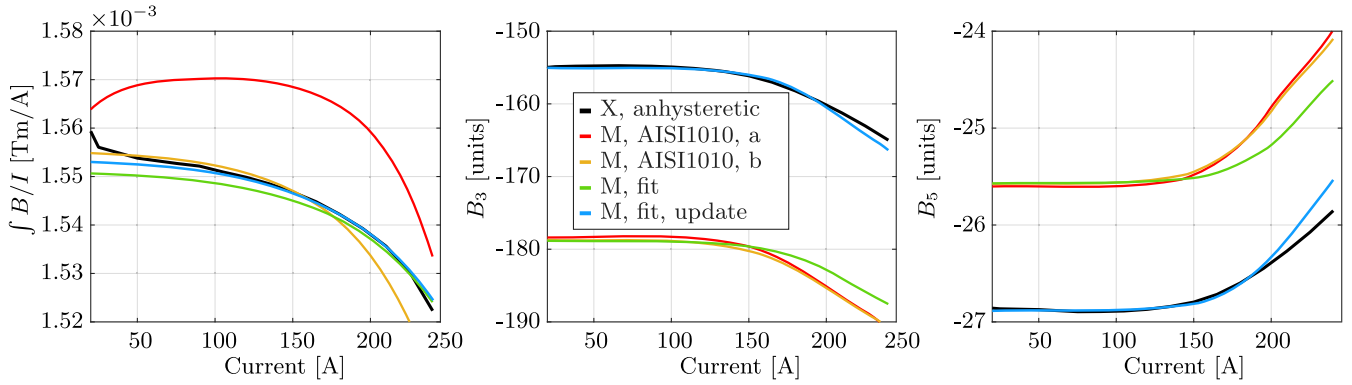

FIG. 5. Integral quantities as a function of the excitation current of the MDX magnet. The letter X denotes the experimental quantity (measurements) and M the different iterations of the model.

personal desktop computer (Intel i7, 32 GB of RAM), ODE45 from MATLAB® takes about 600 s to simulate the anhysteretic behavior of the magnet from 0 to 240 A, which is the maximum excitation current. The model of the measurement system is already available from Ref. [49], so that it is possible to predict the measured quantities from the rotating-coil magnetometer. In order to guarantee a reasonable starting point, other curves for AISI1010 from Ref. [48] were evaluated, and the most suitable one was taken as the initial condition (later identified by the letter b). The Wlodarski curve [Eq. (6)] is adopted, and the fitted parameters are given in Table II.

The effect of the fitting parameters on the flux linked with the excitation coil is shown in Fig. 4. After this step, the magnetization is updated. Measurements of the field harmonics were performed with $r_0 = 0.03$ m, spanning ± 0.75 m on the magnet axis. In the simulation, 60 angular positions for the coil are considered. The multipoles to be corrected in the model are the ones larger than 10^{-4} relative to the main-field level, i.e., $n \in [1, 3, 5]$. The optimization from Eq. (10) is performed at different currents. On average, the integral dipole field must be increased by 15 units and $\mathcal{C}_3$ reduced by 25 units, while $\mathcal{C}_5$ is to be reduced by two units. Results on the magnetization distribution are shown for 200 A in Fig. 6. The correction is mainly in the poles, where the iron saturation is highest. The implementation of $\Delta \boldsymbol{M}(I)$ in the model equations is performed acting on the input matrix $\boldsymbol{F}$, correcting it with values in the nonsaturated regime. A reasonable trade-off is found in the solution $\Delta \boldsymbol{F}(I) = \Delta \boldsymbol{F}(60A)\ \forall\ I$. The effects of the correction is shown in Fig. 5.

A final assessment is undertaken to evaluate the proposed procedure. The modeling, parameter estimation, and updating processes rely only on integral measurements. Independent measurements with a short coil magnetometer yielding a 3D field map [19] can be compared with the updated model. The 3D field map allows to extract the local multipoles at $r_0 = 18$ mm and 240 A. The nonupdated and

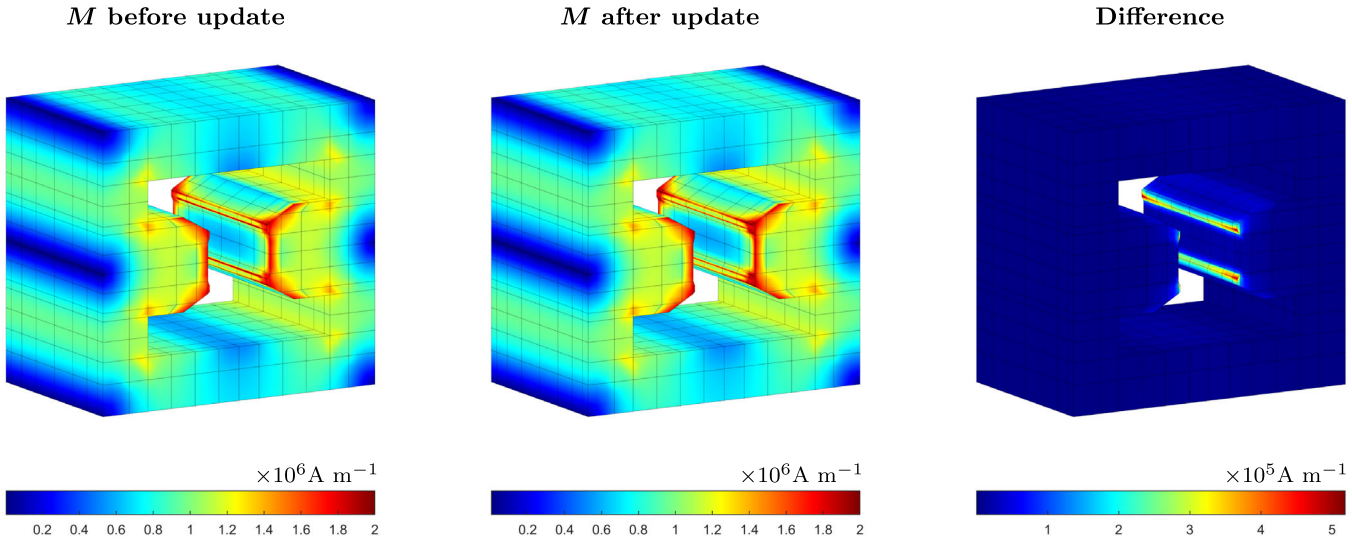

FIG. 6. Magnetization update for 200 A. The magnetization distribution before (left) and after (center) the updating is shown. The absolute difference is also shown (right).

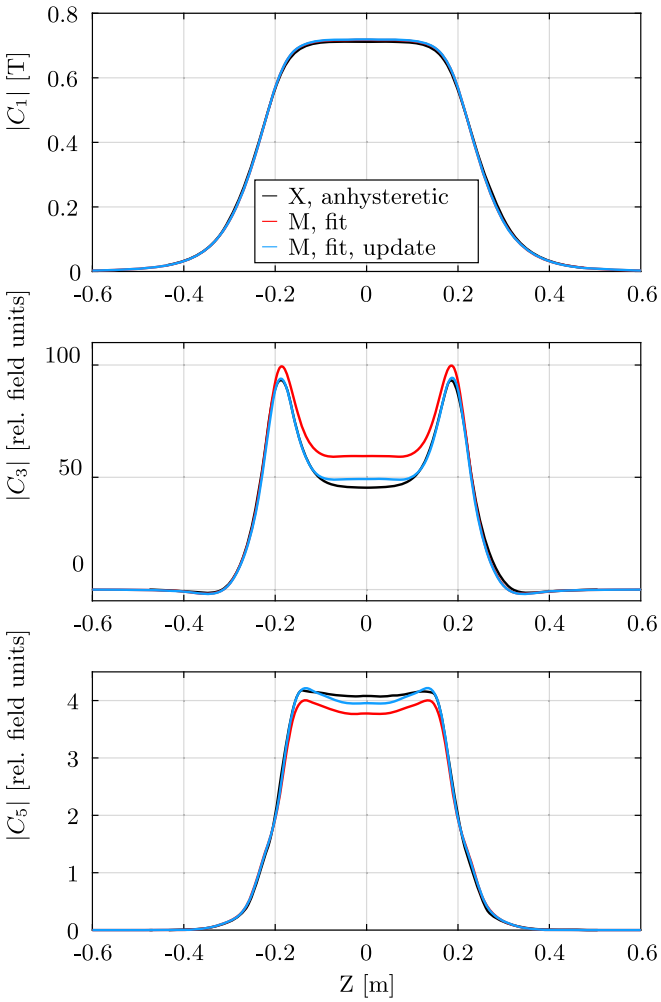

FIG. 7. Multipole profile on magnet axis, from validation measurements. A small rotating coil scanned the magnet on its axis, with $r_0 = 18$ mm. $|C_3|$ and $|C_5|$ are given in *relative field units*, which is the magnitude of the multipole at r_0, divided by the main component $|C_1|$ and multiplied by 10^4.

updated models can then be compared with the results from the map; see Fig. 7. The updated model better replicates the measurements, especially inside the magnet.

V. CONCLUSIONS

This work proposes a combination of simulations and measurements in a data-driven model of normal-conducting magnets. A nonlinear numerical model of the magnet is first established. Magnetic measurements of integral quantities are then performed and employed in a two-step correction procedure. The result is a model which retains its main physical and numerical properties (full order, symmetry, and positive-definiteness of its matrices) while better matching the magnetic measurements. The presented results are meant to be the first step in a wider development of data-driven simulation tools. This is because particle accelerators would greatly benefit from an improved and reliable magnet model, for diagnostic purposes, performance evaluation, operations, and more sophisticated control architectures. The work presents the first step toward a digital twin [50–52] for normal-conducting magnets.

APPENDIX: INTEGRALS FOR THE ASSEMBLY OF MAGNETIZATION VOLUME INTEGRAL METHOD

Equation (2) contains four terms that must be computed. For the facet shape functions, every term on the numerator can be brought outside the integral. The resulting integral can be solved as a double volume integral of $1/r$. In the case of mixed integrals of facets and recirculating shape functions, it is always possible to reorder the integration so that the recirculating function is outside the inner integral. This allows one to solve the inner analytically and the outer numerically, as discussed in Ref. [6]. In case of two recirculating shape functions combined, both $\boldsymbol{p}_j$ and $\boldsymbol{w}_i$ are of this kind; thus, further development is required to deal with the singularity. Only one of the four integrals in Eq. (2) is nonzero, because recirculating shape functions are divergence-free. Considering that each element is divided into faces, the integral is

$$-\frac{1}{4\pi}\sum_{i=1}^{6}\sum_{j=1}^{6}\int_{\mathscr{A}_i}(\boldsymbol{p}_i\cdot\boldsymbol{n})\int_{\mathscr{A}'_j}\frac{(\boldsymbol{w}'_j\cdot\boldsymbol{n}')}{r}\mathrm{dA}'_i\mathrm{dA}_j. \tag{A1}$$

The inner integral has an analytical solution even for singular functions, while the outer one can be solved numerically by Gauss quadrature. The core of the proposed method is the fact that $(\boldsymbol{w}'_j\cdot\boldsymbol{n}')$ is linear in a certain direction on each face. In fact, the recirculating functions are written so that the normal component of $\mathbf{M}$ is linearly changing in one of the perpendicular directions (for instance, the normal component of the two functions on a face parallel to s_1 will be $a\cdot s_2$ and $a\cdot s_3$, where a is a coefficient that depends on the dimensions of the face of the real element). In theory, this statement holds only if the real element is transformed from the reference element by an affine transformation, but in practice also asymptotically affine elements produce a reliable approximation [53,54].

It is, therefore, possible to identify a direction on the face which is parallel to the direction of $(\boldsymbol{w}'_k\cdot\boldsymbol{n}')$. Changing the coordinate system so that x' is parallel to this direction and z' is the outward normal of the face, it is possible to write for each face

$$-\frac{1}{4\pi}a_j\cdot\int_{\mathscr{A}_i}(\boldsymbol{p}_k\cdot\boldsymbol{n})\int_{\mathscr{A}'_j}\frac{x'}{r}\mathrm{d}x'\mathrm{d}y'|\det(J)_{\mathrm{face}}|\mathrm{dA}_i. \tag{A2}$$

If we identify as $(\hat{x}',\hat{y}',\hat{z}')$ the coordinates of each Gauss point on the target surface $\mathscr{A}_i$, we can write the inner integral as

$$\int_{\mathscr{A}'_j} \frac{x' - \hat{x}' + \hat{x}'}{\sqrt{(x' - \hat{x}')^2 + (y' - \hat{y}')^2 + (z' - \hat{z}')^2}} \mathrm{d}x'\mathrm{d}y', \quad \text{(A3)}$$

which can be split in two integrals. The first is written as

$$\int_{\mathscr{A}'_j} \frac{\partial \sqrt{(x' - \hat{x}')^2 + (y' - \hat{y}')^2 + (z' - \hat{z}')^2}}{\partial x'} \mathrm{d}x'\mathrm{d}y', \quad \text{(A4)}$$

where the partial derivative is integrated into x', removing the singularity. The analytical solution is trivial for rectangular faces, solving first the integration in x' and then in y':

$$\int_{y_1}^{y_2} \sqrt{(x'_k - \hat{x}')^2 + (y' - \hat{y}')^2 + (z' - \hat{z}')^2} \mathrm{d}y' = F(x'_k, y)\Big|_{y_1}^{y_2}, \quad \text{(A5)}$$

for $k = 1, 2$.

In the case of parallelogram-shaped faces, it is necessary to divide the domain into subdomain so that the extrema for the inner integration are of the form $x'_k = m_k y' + q_k$. The solution in x' is

$$\int_{y_1}^{y_2} \sqrt{(m_k y' + q_k - \hat{x}')^2 + (y' - \hat{y}')^2 + (z' - \hat{z}')^2} \mathrm{d}y', \quad \text{(A6)}$$

for $k = 1, 2$, which can be solved analytically.

Finally, the second integral term from Eq. (A3) becomes

$$\hat{x}' \int_{\mathscr{A}'_j} \frac{1}{\sqrt{(x' - \hat{x}')^2 + (y' - \hat{y}')^2 + (z' - \hat{z}')^2}} \mathrm{d}x'\mathrm{d}y', \quad \text{(A7)}$$

which can be solved analytically like the integrals for the facet functions.

[1] S. Russenschuck, *Field Computation for Accelerator Magnets: Analytical and Numerical Methods for Electromagnetic Design and Optimization* (Wiley, New York, 2011).

[2] J. Tanabe, *Iron Dominated Electromagnets: Design, Fabrication, Assembly and Measurements* (World Scientific, Singapore, 2005).

[3] G. Moritz, in *Proceedings of the CERN Accelerator School CAS 2009: Specialised Course on Magnets, Bruges, 2009*, http://cds.cern.ch/record/1335027.

[4] L. Bottura and K. Henrichsen, CERN technical report, 2002.

[5] L. Walckiers, in *Proceedings of the CERN Accelerator School CAS 2009: Specialised Course on Magnets, Bruges, 2009* (unpublished). For higher-resolution figures, see https://cds.cern.ch/record/1158462?ln=en.

[6] S. Sorti, C. Petrone, S. Russenschuck, and F. Braghin, Nucl. Instrum. Methods Phys. Res., Sect. A **1011**, 165571 (2021).

[7] M. Polis and R. Goodson, Proc. IEEE **64**, 45 (1976).

[8] A. Berman and E. Nagy, AIAA J. **21**, 1168 (1983).

[9] B. N. Datta, Mech. Syst. Signal Process. **16**, 83 (2002).

[10] J. H. Lim, D.-S. Hwang, D. Sohn, and J.-G. Kim, Aerosp. Sci. Technol. **54**, 59 (2016).

[11] J. Mottershead and M. Friswell, J. Sound Vib. **167**, 347 (1993).

[12] F. Perrin, B. Sudret, and M. Pendola, in *Congrès Français de Mécanique* (AFM, Maison de la Mécanique, 39/41 rue Louis Blanc-92400 Courbevoie, 2007).

[13] K.-V. Yuen and S.-C. Kuok, Appl. Mech. Rev. **64**, 010802 (2011).

[14] D. González, A. Badías, I. Alfaro, F. Chinesta, and E. Cueto, Comput. Methods Appl. Mech. Eng. **326**, 679 (2017).

[15] J. Ching, J. L. Beck, and K. A. Porter, Prob. Eng. Mech. **21**, 81 (2006).

[16] D. Calvetti and E. Somersalo, Computat. Stat. **10**, e1427 (2018).

[17] M. Liebsch, S. Russenschuck, and S. Kurz, IEEE Trans. Magn. **56**, 1 (2020).

[18] A. Lazzaro, F. Cappuzzello, A. Cunsolo, M. Cavallaro, A. Foti, S. Orrigo, M. Rodrigues, J. Winfield, and M. Berz, Nucl. Instrum. Methods Phys. Res., Sect. A **602**, 494 (2009).

[19] G. Ion, M. Liebsch, A. Simona, D. Loukrezis, C. Petrone, S. Russenschuck, H. De Gersem, and S. Schops, Nucl. Instrum. Methods Phys. Res., Sect. A **1011**, 165580 (2021).

[20] A. Canova and M. Repetto, IEEE Trans. Magn. **37**, 1070 (2001).

[21] L. Kettunen and L. R. Turner, IEEE Trans. Magn. **28**, 1639 (1992).

[22] M. Koizumi and Y. Higuchi, IEEE Trans. Magn. **31**, 1516 (1995).

[23] R. Albanese, E. Coccorese, R. Martone, G. Miano, and G. Rubinacci, IEEE Trans. Magn. **27**, 3990 (1991).

[24] R. Albanese and G. Rubinacci, IEEE Trans. Magn. **28**, 1228 (1992).

[25] M. d'Aquino, G. Rubinacci, A. Tamburrino, and S. Ventre, IEEE Trans. Magn. **49**, 3167 (2013).

[26] P. B. Bochev and D. Ridzal, SIAM J. Numer. Anal. **47**, 487 (2009).

[27] T.-T. Nguyen, G. Meunier, J.-M. Guichon, O. Chadebec, and T.-S. Nguyen, IEEE Trans. Magn. **50**, 549 (2014).

[28] G. Meunier, O. Chadebec, J.-M. Guichon, V. Le-Van, J. Siau, B. Bannwarth, and F. Sirois, IEEE Trans. Magn. **52**, 1 (2015).

[29] V. Le-Van, G. Meunier, O. Chadebec, and J.-M. Guichon, IEEE Trans. Magn. **51**, 1 (2015).

[30] B. Krstajic, Z. Andelic, S. Milojkovic, S. Babic, and S. Salon, IEEE Trans. Magn. **28**, 1088 (1992).

[31] S. F. Matringe, *Mixed Finite Element Methods for Discretization and Streamline Tracing* (Stanford University, Stanford, 2008).

[32] J. Leite, N. Sadowski, P. Kuo-Peng, N. Batistela, J. Bastos, and A. de Espindola, IEEE Trans. Magn. **40**, 1769 (2004).

[33] H. De Gersem, I. Munteanu, and T. Weiland, IEEE Trans. Magn. **44**, 710 (2008).

[34] Z. Włodarski, Physica (Amsterdam) **373B**, 323 (2006).

[35] E. Kokornaczyk and M. W. Gutowski, IEEE Trans. Magn. **51**, 1 (2014).
[36] U. Römer, https://tuprints.ulb.tu-darmstadt.de/4950/1/diss_main_vf.pdf.
[37] F. Fiorillo, Metrologia **47**, S114 (2010).
[38] D. Chatterjee, IEEE Transactions on Industrial Electronics **58**, 5336 (2011).
[39] K. Wang, W. Yao, B. Chen, G. Shen, K. Lee, and Z. Lu, IEEE Transactions on Industrial Electronics **62**, 2144 (2015).
[40] Y. Paquay, O. Brüls, and C. Geuzaine, IEEE Trans. Magn. **52**, 1 (2016).
[41] Z. Xu, X. Lin, H. Zhuang, B. Jiang, H. Lou, and J. He, in *Proceedings of the 2011 9th IEEE International Conference on ASIC* (IEEE, New York, 2011), pp. 886–889.
[42] E. Cueto, F. Chinesta, and A. Huerta, in *Separated Representations and PGD-Based Model Reduction* (Springer, New York, 2014), pp. 1–26.
[43] Y. Liang, H. Lee, S. Lim, W. Lin, K. Lee, and C. Wu, J. Sound Vib. **252**, 527 (2002).
[44] T. Bui-Thanh and M. Damodarany, in *Proceedings of the 21st AIAA Applied Aerodynamics Conference, Orlando, Florida, 2003*, 10.2514/6.2003-4213.
[45] O. Chadebec, J.-L. Coulomb, and F. Janet, IEEE Trans. Magn. **42**, 515 (2006).
[46] R. Lopez and J. R. Anglada, IEEE Trans. Appl. Supercond. **30**, 1 (2020).
[47] S. Sorti, C. Petrone, S. Russenschuck, and F. Braghin, *Proceedings of the 22nd International Workshop on ADC and DAC Modelling and Testing IMEKO TC-4 2020 Palermo, Italy, 2020* (2020), https://www.imeko.org/publications/tc4-2020/IMEKO-TC4-2020-38.pdf.
[48] S. Sgobba, arXiv:1103.1069.
[49] S. Sorti, C. Petrone, S. Russenschuck, and F. Braghin, Acta IMEKO **10**, 30 (2021).
[50] E. Glaessgen and D. Stargel, in *Proceedings of the 53rd AIAA/ASME/ASCE/AHS/ASC Structures, Structural Dynamics and Materials Conference 20th AIAA/ASME/AHS Adaptive Structures Conference 14th AIAA* (American Institute of Aeronautics and Astronautics, Reston, VA, 2012), p. 1818.
[51] D. Jones, C. Snider, A. Nassehi, J. Yon, and B. Hicks, CIRP J. Manufact. Sci. Technol. **29**, 36 (2020).
[52] F. Chinesta, E. Cueto, E. Abisset-Chavanne, J. L. Duval, and F. El Khaldi, Arch. Comput. Methods Eng. **27**, 105 (2020).
[53] D. N. Arnold, D. Boffi, and R. S. Falk, SIAM J. Numer. Anal. **42**, 2429 (2005).
[54] D. Boffi, Applied Numerical Mathematics **56**, 1271 (2006).